Raman spectroscopy of two novel semiconductors and related superlattices: Cubic $Cd_{1-x}Mn_xSe$ and $Cd_{1-x}Zn_xSe$

R. G. Alonso, E.-K. Suh, and A. K. Ramdas
Department of Physics, Purdue University, West Lafayette, Indiana 47907-1301

N. Samarth, H. Luo, and J. K. Furdyna
Department of Physics, University of Notre Dame, Notre Dame, Indiana 46556

(Received 1 May 1989)

The Raman scattering from $Cd_{1-x}Zn_xSe$ and $Cd_{1-x}Mn_xSe$, grown by molecular-beam epitaxy on (001) GaAs substrates, shows zone-center optical phonons characteristic of a zinc-blende structure, indicating that these epilayers represent the cubic phase of these materials which in the bulk crystallize only in the wurtzite form. The variation of the frequency of the zone-center optical phonons as a function of composition x shows a "two-mode" behavior in $Cd_{1-x}Mn_xSe$ and a pattern intermediate between "two-mode" and "one-mode" in $Cd_{1-x}Zn_xSe$. The modified–random-element–isodisplacement model provides a satisfactory basis for these patterns. In the case of $Cd_{1-x}Mn_xSe$, the large Raman shifts associated with the spin flip of donor-bound electrons and the huge Zeeman shifts of an excitonic component observed in photoluminescence (including saturation at high magnetic fields and low temperatures), show that the large *sp-d* exchange interaction characteristic of diluted magnetic semiconductors is manifested also in the zinc-blende phase of this alloy.

I. INTRODUCTION

The tetrahedrally coordinated II-VI compound semiconductors typically occur in the cubic (zinc-blende) or the hexagonal (wurtzite) structure.[1] Indeed, some of the Mn-based II-VI-compound diluted magnetic semiconductors[2] (DMS) grown by bulk crystal-growth techniques may occur in the zinc-blende phase over a certain range of composition and in the wurtzite phase outside that range. For instance, $Zn_{1-x}Mn_xSe$ is zinc blende for $0 \le x \le 0.35$ and wurtzite for $0.35 < x \le 0.55$. On the other hand, $Cd_{1-x}Mn_xSe$ occurs in the wurtzite phase throughout the composition range accessible to bulk growth techniques ($0 \le x \le 0.5$). Recently, Samarth *et al.*[3,4] have demonstrated that CdSe,[5] $Cd_{1-x}Mn_xSe$, and $Cd_{1-x}Zn_xSe$ can be stabilized in the cubic *zinc-blende* structure by growing epitaxial layers on (001) GaAs substrates using molecular-beam epitaxy (MBE). This exciting development has several implications of fundamental importance. First, it permits the study of the physical properties of these materials in the previously inaccessible zinc-blende phase and enables us to examine the relationship between the properties of MBE-grown cubic and bulk-grown hexagonal structures. Further, it offers the possibility of fabricating new types of DMS superlattices such as $Cd_{1-x}Mn_xSe/Cd_{1-y}Zn_ySe$ in which appropriate choices of x and y can lead to *lattice-matched* wells and barriers and $ZnSe/Cd_{1-x}Mn_xSe$ superlattices with magnetic wells. Finally, the relative ease of growing *n*-type CdSe and $Cd_{1-x}Mn_xSe$ in the bulk also augurs well for attempts at fabricating lattice-matched heterostructures such as (*p*-type ZnTe)/(*n*-type CdSe) and modulation-doped superlattices such as CdSe/(*n*-type $Cd_{1-x}Mn_x$ Se).

The vibrational spectra of mixed crystals are of special interest as they illustrate many fundamental aspects of lattice vibrations.[6] The Raman spectra of the tetrahedrally coordinated II-VI compound semiconductor alloys such as $Cd_{1-x}Mn_xTe$ and $Cd_{1-x}Zn_xTe$ provide excellent illustrations of the lattice dynamics of mixed crystals. In this connection, the Raman spectroscopy of cubic CdSe, $Cd_{1-x}Mn_xSe$, and $Cd_{1-x}Zn_xSe$ is also of interest. Furthermore, as a new member of the DMS family of alloys, cubic $Cd_{1-x}Mn_xSe$ is very appealing for a study of its magnetic properties. We note here that DMS alloys display a host of striking magnetic phenomena such as giant Faraday rotation[7] and spin-flip Raman scattering[8] associated with donor-bound electrons, as well as that arising from the Zeeman multiplet of the ground state of the magnetic ion. The underlying spin-spin exchange between the *d* electrons of Mn^{2+} and the *s* electrons of the Γ_6 conduction band and the *p* electrons of the Γ_8 valence band (the so-called *sp-d* exchange) can now be explored in cubic $Cd_{1-x}Mn_xSe$.

In the present paper, we report the results of our study of the Raman spectra of the epilayers of cubic CdSe, $Cd_{1-x}Mn_xSe$, and $Cd_{1-x}Zn_xSe$, as well as of two "attempted" superlattices: $Cd_{1-x}Zn_xSe/Cd_{1-x}Mn_xSe$ and $ZnSe/Cd_{1-x}Mn_xSe$. We first describe the photoluminescence spectra of zinc-blende CdSe, $Cd_{1-x}Mn_xSe$, and $Cd_{1-x}Zn_xSe$—this allows us to estimate their band-edge parameters E_g and the effective *g* factor of the band electrons. We then discuss the vibrational Raman spectra of these epilayers, and show that these spectra confirm the cubic structure of these systems. Finally, we discuss Raman scattering from magnetic excitations in $Cd_{1-x}Mn_xSe$ and in the two superlattices mentioned above.

II. EXPERIMENTAL PROCEDURE

The epilayers used in this study were grown by molecular-beam epitaxy (MBE) on (001) GaAs substrates. The epilayer thickness ranged from 0.3 to 3.7 μm. The lattice parameter (and therefore the composition) of the samples were determined by x-ray diffraction. The epilayers were found to be of zinc-blende structure, with a (001) layer plane (the growth direction is designated by z in this paper).

Raman spectra were excited with monochromatic radiation from Kr^+ or Ar^+ lasers, or from a tunable ring dye laser operated with DCM.[9] The power of the incident beam was typically ≤ 75 mW in order to avoid sample heating. Measurements in an external magnetic field were carried out using a variable temperature (1.8–300 K) optical cryostat with a superconducting coil providing external magnetic fields up to 60 kG. Scattered light was spectrally analyzed with a computer-controlled double (triple) Spex Industries, Inc. monochromator and detected with standard photon counting electronics. The photoluminescence measurements were carried out on the same spectrometer.

III. RESULTS AND DISCUSSION

A. Photoluminescence

The photoluminescence spectra obtained during our Raman scattering study of $Cd_{1-x}Zn_xSe$ and $Cd_{1-x}Mn_xSe$ allowed us to establish the resonance conditions for Raman scattering. In addition, estimates of the fundamental energy gap and the effective g factors characterizing the band extrema could be obtained from these measurements. In this section we focus on the photoluminescence spectra and their interpretation.

1. CdSe

The photoluminescence spectrum of an epilayer of cubic CdSe is shown in Fig. 1. We ascribe the peak labeled A to an exciton bound to a shallow center, in view of its proximity to the energy gap determined from the piezomodulated reflectivity[3] spectrum (see Table I). As we shall see in Sec. III B, the LO-phonon Raman line in cubic CdSe is at 213 cm^{-1}. The energy separation between the luminescence peaks B and C and that between D and E, are close to the energy of the LO phonon, strongly suggesting that C and E are phonon replicas of B and D. (Phonon replicas such as these are commonly observed in the luminescence spectra of CdTe.[10]) Peaks B, D, and F are presumably due to impurity emission centers yet to be identified.

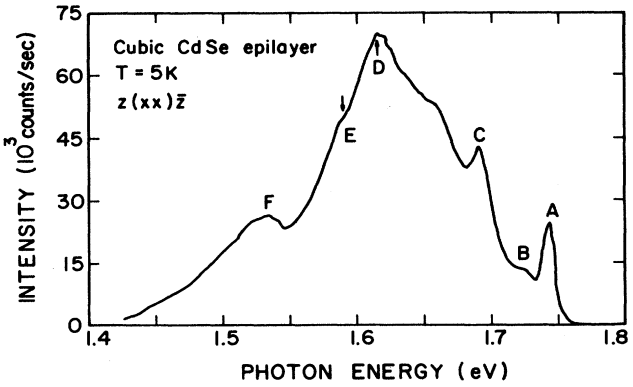

FIG. 1. The photoluminescence spectrum of an epilayer of cubic (zinc-blende) CdSe at $T=5$ K with incident laser wavelength of 6764 Å.

The energy band structure of wurtzite CdSe is well documented in the literature,[11] but there is only very limited information about cubic CdSe. The piezomodulated reflectivity study carried out in our group[3] yielded a value of 1.75 eV for the fundamental gap at $T=10$ K, in excellent agreement with that obtained from photoluminescence spectrum. In Table I we compare the energies of the fundamental gap transitions in cubic and wurtzite CdSe at several temperatures. The subindices A and B for the energy gap in the wurtzite crystal correspond to the A and B valence bands resulting from the anisotropic part of the crystal potential in the hexagonal structure; the energy gap for the cubic structure is smaller by 0.7 eV than that for the hexagonal structure. It is interesting to note that for the closely analogous II-VI compound semiconductors CdS and ZnS, the energy gaps reported in the literature[12] are smaller for the cubic as compared to those of the hexagonal structure. The current band-structure calculations on II-VI compound semiconductors which occur either in the zinc-blende or wurtzite structure do not provide sufficient insight into the nature of the difference in energy gap. Calculations based on the orthogonalized-plane-wave (OPW) method[13] applied to cubic CdSe yielded a direct gap of 1.9 eV, which exceeds the experimental value by 0.15 eV. Also, the energy gaps for the wurtzite[14] as compared to that of the zinc blende,[13] calculated either by the OPW or the pseudopotential techniques, yielded a larger value for the wurtzite in agreement with experimental results in CdSe, CdS, and ZnS.[12] This, however, has to be taken cautiously because, in general, the same calculations were not available for both the cubic and the hexagonal structures. It appears that before any general conclusion can be derived, band-structure calculations must be performed using ex-

TABLE I. Excitonic energies (in eV) in wurtzite and zinc-blende CdSe. See the text for the labels of the excitonic transitions.

	$T=300$ K	$T=80$ K	$T=10$ K
		Wurtzite[a]	
E_A	1.74	1.81	1.82
E_B	1.77	1.83	1.84
		Zinc-blende[b]	
E_A	1.67	1.74	1.75

[a]See Ref. 11.
[b]See Ref. 3.

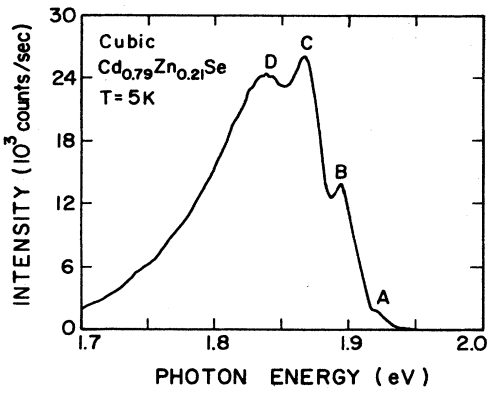

FIG. 2. The photoluminescence spectrum of a cubic (zinc-blende) epilayer of $Cd_{1-x}Zn_xSe$ ($x=0.21$) at $T=5$ K. The 5145-Å radiation from an Ar^+ laser excited the photoluminescence.

actly the same theoretical approach for both structures in the crystals of interest, e.g., CdSe, ZnSe, and MnSe.

2. $Cd_{1-x}Zn_xSe$

Figure 2 shows the photoluminescence spectrum of $Cd_{1-x}Zn_xSe$, $x=0.21$, where four peaks (A, B, C, and D) are clearly distinguished. The energy of A at $x=0$ is lower by 56 meV than that of the free exciton observed in the piezomodulated reflectivity spectrum of CdSe (see Table I). We therefore attribute A to a shallow emission center and B, C, and D to its optical phonon replicas. In Fig. 3 we plot the energy of the photoluminescence feature at A as a function of x. As can be seen, the x dependence of this feature is approximately linear, again consistent with the virtual-crystal approximation.

3. $Cd_{1-x}Mn_xSe$

It is possible to grow cubic $Cd_{1-x}Mn_xSe$ by MBE in which Mn^{2+} has randomly replaced Cd. We once more emphasize that bulk $Cd_{1-x}Mn_xSe$ has wurtzite structure. As in cubic CdSe, one observes a peak close to the free-exciton signature in the piezomodulated reflectivity in the photoluminescence spectrum of cubic $Cd_{0.9}Mn_{0.1}Se$ and can also be attributed to an exciton bound to a shallow center. If one assumes a linear x dependence of this exciton energy (as indicated by the solid straight line in Fig. 4 and as justified in the virtual-crystal approximation), one sees that its energy tracks the energy gap as a function of x. Figure 4 also shows that, throughout the composition range, the energy gap of the cubic $Cd_{1-x}Mn_xSe$ for a given x is smaller than that of the corresponding hexagonal structure. Piezomodulated reflectivity measurement data presented in Table I show a similar difference in the energy of the A exciton of the cubic and of the hexagonal CdSe ($x=0$). The concentration range over which the position of the bound exciton can be followed is limited by the occurrence of the photoluminescence feature associated with the 2.2-eV internal transition of the Mn^{2+} ion; when the excitonic feature occurs close to the Mn^{2+} luminescence or beyond, the strong Mn^{2+} luminescence dominates the spectrum, preventing the observation of the excitonic feature of $Cd_{1-x}Mn_xSe$ for $x>0.4$. We add parenthetically that the piezomodulated reflectivity measurements do not suffer from this limitation.

In DMS's, the *sp-d* exchange interaction between band

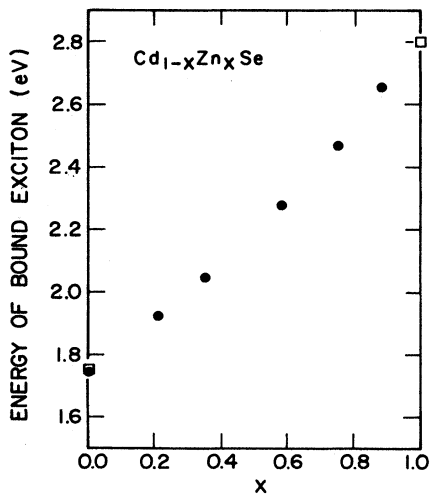

FIG. 3. Position of the photoluminescence peaks in zinc-blende $Cd_{1-x}Zn_xSe$ as function of the Zn concentration x at $T=5$ K. The points indicated with a square at $x=0$ and $x=1$ were obtained from piezomodulated reflectivity measurements of the A exciton in CdSe and ZnSe at $T=10$ K.

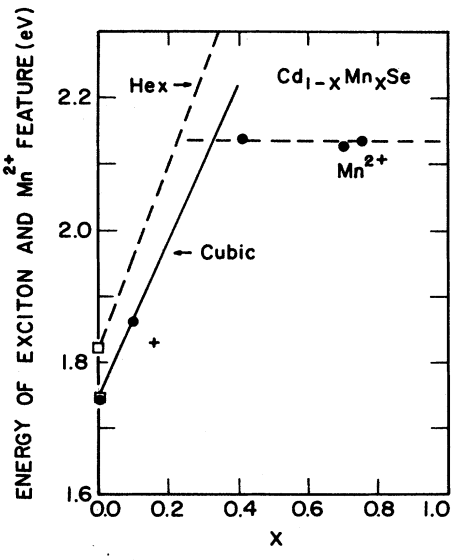

FIG. 4. Position of the photoluminescence peak of the donor-bound exciton in zinc-blende $Cd_{1-x}Mn_xSe$ as function of Mn^{2+} concentration x. For comparison, the energy gap of the wurtzite structure as a function of x (observed in bulk crystals) is shown by the dashed line. The horizontal line denotes the onset of the 2.2-eV Mn^{2+} photoluminescence.

electrons and the $3d$ subshell of the Mn^{2+} ions results in the large spin splitting of the $J=\frac{1}{2}$ conduction band and the $J=\frac{3}{2}$ valence band in the presence of an external magnetic field. It is of interest to compare the magnitude of these Zeeman splittings in the wurtzite and cubic structures of $Cd_{1-x}Mn_xSe$. Figure 5 shows the photoluminescence shift with magnetic field in cubic $Cd_{1-x}Mn_xSe$, $x=0.16$, at $T=5$ K. The crystal was excited with the 4579-Å line with a power of 10 mW. The photoluminescence spectra were obtained with an external magnetic field in the range 0–60 kG parallel to the plane of the epilayer. The large Zeeman shift and the saturation at high magnetic field are clearly seen. The position of the photoluminescence peak corresponds to the Zeeman component of the A exciton formed by the $m_s=-\frac{1}{2}$ component of the conduction band and the $m_s=\frac{3}{2}$ component of the valence band. The shift of this Zeeman component is given by $\Delta E=g\mu_B H$. From the slope of the linear portion of the curve in Fig. 5 we obtain a g factor of 160 at 5 K; this large g factor is typical of DMS's. The corresponding g factor for hexagonal $Cd_{1-x}Mn_xSe$ at $T=5$ K for a comparable x estimated from the results given in Ref. 15 is $g_{\text{hex}}\sim 200$, somewhat larger than that for the cubic structure. The magnitude of the Zeeman shift with magnetic field is given by $\Delta E=\frac{1}{2}N_0(\alpha-\beta)x\langle S\rangle$, where α and β are the conduction- and valence-band exchange integrals and $\langle S\rangle$ is the magnitude of the thermal average of Mn^{2+} spins.[8] The difference in the g factors could be attributed to different values of α and β for the cubic structure. Since Mn^{2+} in the cubic structure has the same number of nearest neighbors as in the wurtzite structure, one expects comparable α and β for the cubic and the hexagonal structures. Before any significance can be attached to these differences, it is of interest to carry out spin-flip studies which will, in combination with the above results, allow an independent determination of the magnitude of both exchange constants.

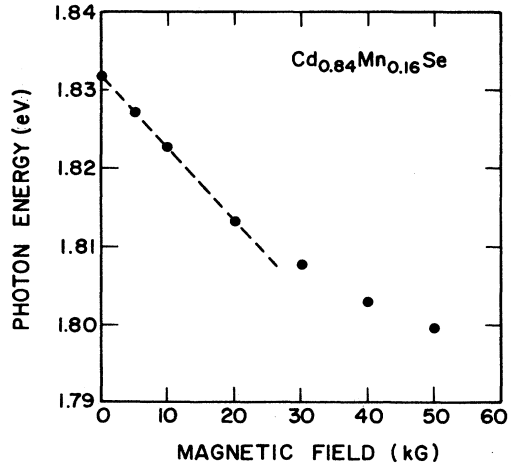

FIG. 5. Position of the photoluminescence peak as a function of magnetic field in zinc-blende $Cd_{1-x}Mn_xSe$, $x=0.16$, at $T=5$ K.

B. Vibrational Raman spectra

In this subsection we present a Raman-scattering study of the vibrational modes of cubic $Cd_{1-x}Zn_xSe$ and $Cd_{1-x}Mn_xSe$ epilayers. We note here that, to date, only the Raman spectrum of uniaxial $Cd_{1-x}Mn_xSe$ (including CdSe) and cubic ZnSe have been investigated.[16] The successful growth of cubic $Cd_{1-x}Zn_xSe$ now allows its Raman study over the entire alloy composition range $0\le x\le 1$. Previous Raman scattering studies on $Cd_{1-x}Mn_xSe$ (Ref. 17) were carried out on the hexagonal phase with $0.0\le x\le 0.51$; a comparison of the Raman spectra of the zinc-blende and the wurtzite structures of this alloy is given at the end of this subsection. This Raman study unambiguously proves that these MBE-grown $Cd_{1-x}Zn_xSe$ and $Cd_{1-x}Mn_xSe$ epilayers have cubic zinc-blende structure.

The Raman spectrum of a (001) epilayer of cubic $Cd_{1-x}Zn_xSe$, $x=0.75$, recorded in the backscattering geometry $z(xx)\bar{z}$ is shown in Fig. 6. The spectrum was recorded at $T=5$ K with the 4965-Å line of the Ar^+ laser. The Raman lines labeled LO and TO can be traced to the LO and TO phonons of CdSe as $x\to 0$ and to the LO and TO phonons of ZnSe as $x\to 1.0$. These extrapolations can be appreciated from the frequencies of the relevant Raman lines as a function of x displayed in the right-hand side of Fig. 7 for $Cd_{1-x}Zn_xSe$. In addition to the transverse-optical (TO) phonon and the longitudinal-optical (LO) phonon, there is a Raman peak labeled I which can be traced to the impurity mode of Zn in CdSe at $x=0$ and to the impurity mode of Cd in ZnSe at $x=1$.

The Raman spectrum of a (001) epilayer of cubic $Cd_{1-x}Mn_xSe$, $x=0.16$, recorded in the backscattering geometry $z(xx)\bar{z}$, is shown in Fig. 8. The spectrum was taken at $T=5$ K with the 6328-Å line of a He-Ne laser. As shown in the left-hand side of Fig. 7, the Raman peak labeled LO_2 can be traced to the zone-center LO phonon of CdSe as $x\to 0$. The Raman peak labeled LO_1 corresponds to the line evolving from the local mode of Mn in CdSe as x increases.

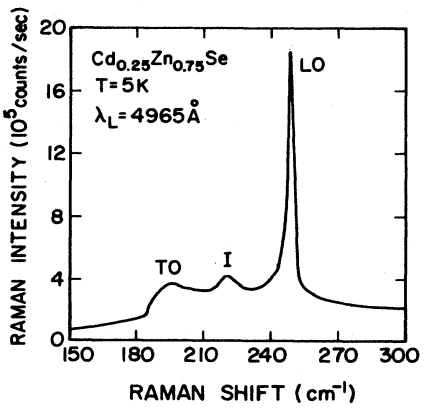

FIG. 6. Raman spectrum of a (001) epilayer of zinc-blende $Cd_{1-x}Zn_xSe$, $x=0.75$, at $T=5$ K. The spectrum was recorded in the backscattering geometry $z(xx)\bar{z}$ with incident wavelength of 4965 Å.

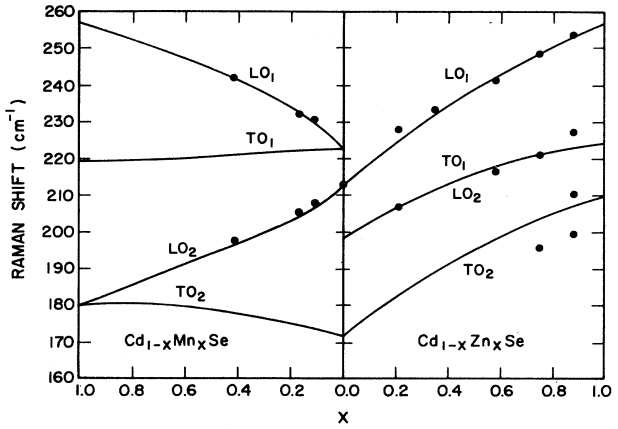

FIG. 7. Composition dependence of the zone-center optical phonon frequencies in zinc-blende $Cd_{1-x}Zn_xSe$ and $Cd_{1-x}Mn_xSe$. The solid lines were calculated with the MREI model for mixed crystals (Ref. 6). The assignments of the modes follow the scheme in Genzel *et al.* (Ref. 18).

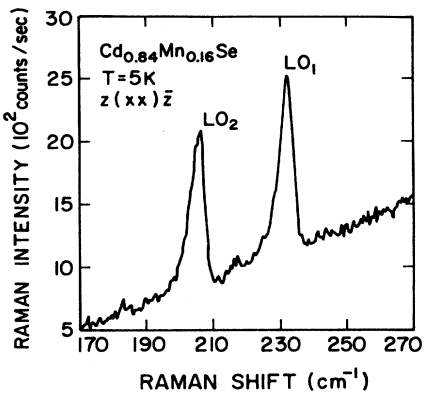

FIG. 8. Raman spectrum of the zinc-blende $Cd_{0.84}Mn_{0.16}Se$ epilayer at $T=5$ K. The spectrum was recorded in the backscattering geometry $z(xx)\bar{z}$ with incident wavelength of 6328 Å.

The observation of the TO mode, as indicated by a number of experimental points in Fig. 7, is rather surprising, since the TO mode is forbidden in the (001) orientation of the epilayers. This could be due to the near-resonant conditions of the Raman experiment and/or a small departure from the backscattering geometry. In this connection we plan to explore epilayers grown on (111) GaAs substrates in the future.

We now focus our attention on Fig. 7. The right-hand side of Fig. 7 shows the so called "intermediate-mode" behavior of cubic $Cd_{1-x}Zn_xSe$. In this case, the impurity mode as $x\rightarrow 0$ is the local impurity mode of Zn in CdSe and evolves into the local mode of Cd in ZnSe as $x\rightarrow 1$. The LO and the TO modes of CdSe evolve into the LO and TO modes of ZnSe, respectively, as $x\rightarrow 1$. In contrast to the intermediate-mode behavior exhibited by the optical phonons in $Cd_{1-x}Zn_xSe$, the optical phonons of $Cd_{1-x}Mn_xSe$ do show a composition dependence corresponding to a "two-mode" behavior. As shown in the left-hand side of Fig. 7, in the two-mode behavior the modes (LO and TO) of each of the two binary crystals involved in the alloy maintain their character throughout the concentration range. We shall refer to them as "CdSe" modes and "ZnSe" modes. The CdSe modes at $x=0$ converge into the gap mode of Cd in MnSe as $x\rightarrow 1$. Similarly, the MnSe modes at $x=1$ become the local mode of Mn in CdSe as $x\rightarrow 0$. At $x=0$ the Mn impurity in CdSe has a higher frequency than the two modes of CdSe, as expected for an impurity with a mass significantly smaller than those of the other constituents. On the other hand, the Zn impurity in CdSe, with a higher mass than Mn, has a lower frequency which falls between the two modes of CdSe. This is, in part, the origin of the dramatic difference in the mode behavior as a function of x in these two mixed crystals.

The curves in Fig. 7 were generated from a modified random-element isodisplacement (MREI) model.[6,18] The fundamental assumptions of the MREI model are that in the long-wavelength limit ($q\sim 0$), the anions and the cations of like species vibrate with the same phase and am-

TABLE II. Parameters in the MREI model. Note: ϵ_0 and a are the notations for the static dielectric constant and lattice constant, respectively.

$Cd_{1-x}Zn_xSe$	$Cd_{1-x}Mn_xSe$
$\omega_{TO(CdSe)}=171.5$ cm^{-1}	
$\omega_{LO(CdSe)}=212.6$ cm^{-1}	
$\omega_{I(CdSe:Zn)}=198.0$ cm^{-1}	$\omega_{I(CdSe:Mn)}=222.5$ cm^{-1}
$\omega_{TO(ZnSe)}=209.9$ cm^{-1}	$\omega_{TO(MnSe)}=219.5$ cm^{-1}
$\omega_{LO(ZnSe)}=256.6$ cm^{-1}	$\omega_{LO(MnSe)}=257$ cm^{-1}
$\omega_{I(ZnSe:Cd)}=224.0$ cm^{-1}	$\omega_{I(MnSe:Cd)}=180.0$ cm^{-1}
$\epsilon_0(CdSe)=9.53$	
$\epsilon_0(ZnSe)=8.80$	$\epsilon_0(MnSe)=10.0$
$a=6.077-0.407x$ Å	$a=6.077-0.175x$ Å
Resultant force constants [10^6 amu (cm^{-1})^2]	
$F_{Cd\text{-}Se}=3.34$,[a] 2.34,[a] $F_{Zn\text{-}Se}=2.16$, $F_{Cd\text{-}Zn}=2.30$	
$F_{Mn\text{-}Se}=2.02$, $F_{Cd\text{-}Mn}=1.30$	

[a]The larger value corresponds to $Cd_{1-x}Zn_xSe$ and the smaller to $Cd_{1-x}Mn_xSe$.

plitude and that the force which each ion experiences is provided by a statistical average of the interaction with its neighbors. The frequency of the vibrational modes in cubic $Cd_{1-x}Zn_xSe$ and cubic $Cd_{1-x}Mn_xSe$ as a function of x (Fig. 7) were determined from the macroscopic parameters[19] listed in Table II. The resulting force constants are also given in the table. For $Cd_{1-x}Zn_xSe$ the magnitude of the second-neighbor force constant required in this calculation turns out to be close to that corresponding to nearest neighbors which may indicate a limitation of the model. As illustrated in Fig. 7, the curves generated from this MREI model follow the experimental curves quite well.

In Fig. 9 we compare the frequencies of the zone-center Raman lines as a function of x observed in cubic and uniaxial[17] $Cd_{1-x}Mn_xSe$. Both structures show a similar two-mode behavior. In the cubic zinc-blende [$F\bar{4}3m$ (T_d^2)] crystals only F_2 optical modes are allowed. In the wurtzite [$P6_3mc$ (C_{6v}^4)] crystals the Raman active zone-center optical phonons consist of $A_1+E_1+2E_2$. The hexagonal crystal field splits the F_2 vibrational modes of the zinc-blende lattice into the A_1 and E_1 modes of the wurtzite structure. Since the frequency of F_2 observed in the zinc-blende epilayers are close to those of A_1 and E_1 in the wurtzite $Cd_{1-x}Mn_xSe$ throughout the composition range (see Fig. 9), we conclude that the anisotropy of the crystal field is small.

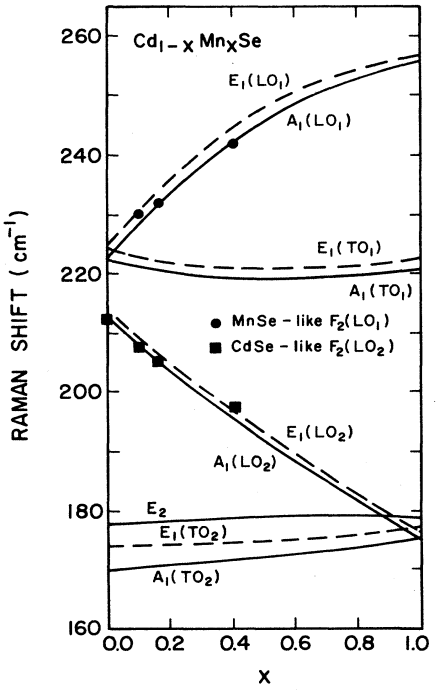

FIG. 9. Composition dependence of the zone-center optical phonon frequencies in $Cd_{1-x}Mn_xSe$ with zinc-blende and wurtzite structures. The solid and dashed lines follow the experimental data for the wurtzite structure (Ref. 17). The experimental points corresponding to the $F_2(LO_1)$ and $F_2(LO_2)$ modes in the cubic structure are close to those of the $A_1(LO)$ and $E_1(LO)$ modes in the hexagonal modification.

TABLE III. Superlattices incorporating zinc-blende $Cd_{1-x}Mn_xSe$ and $Cd_{1-x}Zn_xSe$. d_w is well width, d_b is barrier width, and n is number of periods (d_w+d_b).

Sample	Well	Barrier	d_w/d_b Å	n	Buffer
SL-7	$Cd_{0.9}Zn_{0.1}Se$	$Cd_{0.9}Mn_{0.1}Se$	50/50	100	CdSe
SL-8	$Cd_{0.9}Mn_{0.1}Se$	ZnSe	30/60	100	ZnSe

C. Raman scattering from magnetic excitations

1. *Raman-electron paramagnetic resonance of Mn^{2+}*

In this subsection we present a Raman-scattering study of magnetic excitations in the zinc-blende epilayers of the DMS alloy $Cd_{1-x}Mn_xSe$ and related superlattices. We consider here the magnetic excitations common to the bulk and the superlattices. The nominal parameters of the superlattices investigated are listed in Table III.

In addition to the vibrational modes described in Sec. III B, the Raman spectra of $Cd_{1-x}Mn_xSe$ show magnetic Raman features typically encountered in DMS's. Figure 10 shows the Raman line associated with the spin-flip transition within the Zeeman split $3d^5$ multiplet of Mn^{2+}, i.e., the Raman-EPR (PM), observed in $Cd_{1-x}Mn_xSe$, $x=0.16$, at $T=5$ K. The intensity of this Raman line is resonantly enhanced when the scattered phonon is close to that of a Zeeman component of the excitonic transition. This resonant enhancement demonstrates[20] that the Raman mechanism for Raman EPR involves interband electronic transitions. The Raman-EPR shift, given by $\hbar\omega_{PM}=g_{Mn}\mu_B H$, yields a g factor of 2, as expected for Mn^{2+}.

Figure 11(a) shows the remarkable Raman-EPR spectrum observed in a $Cd_{0.9}Mn_{0.1}Se/ZnSe$ superlattice (SL-8), at $T=5$ K, where $Cd_{0.9}Mn_{0.1}Se$ is the well. The ob-

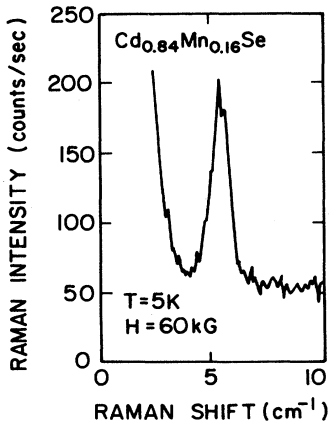

FIG. 10. The Raman-EPR (PM) peak in zinc-blende $Cd_{1-x}Mn_xSe$, $x=0.16$, at $T=5$ K. The spectrum was recorded in the backscattering geometry $z(yx)\bar{z}$ with $H=60$ kG along x and incident wavelength of 6471 Å with 50 mW power.

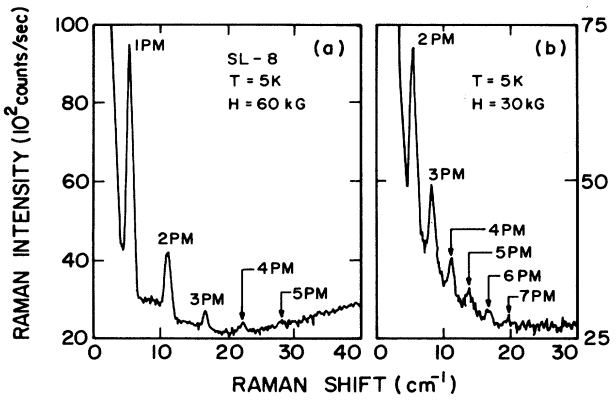

FIG. 11. Raman-EPR lines in the $Cd_{0.9}Mn_{0.1}Se/ZnSe$ superlattice (SL-8), at $T=5$ K. The Raman lines in (a) correspond to 1PM, 2PM, 3PM, 4PM, and 5PM. They result from transitions within the Zeeman multiplet of Mn^{2+}, with $\Delta m_S=1$, 2, 3, 4, and 5, respectively. This spectrum is obtained in the crossed polarization $z(yx)\bar{z}$ with magnetic field $H=60$ kG along x and incident wavelength of 6764 Å with 57 mW power. The 5PM line appearing superposed on the photoluminescence shows how closely the resonance condition is fulfilled. The spectrum in (b) shows the additional 6PM and 7PM lines observed at a lower magnetic field. In this spectrum the 1PM line is obscured by the parasitic laser light.

served Raman lines labeled 1PM, 2PM, 3PM, 4PM, and 5PM have their origin in the transitions with $\Delta m_S=1$, 2, 3, 4, and 5 within the $J=\frac{5}{2}$ Zeeman multiplet of Mn^{2+}. Figure 12 shows the linear dependence of the Raman-EPR shift as function of magnetic field where the solid lines correspond to $g_{Mn^{2+}}=2$. In Fig. 11(b) we also observe peaks corresponding to 6PM and 7PM (see also Fig. 12). The multiple spin-flip features in a DMS can be accounted for in terms of excitations within neighboring pairs of Mn^{2+} ions coupled antiferromagnetically and assuming an anisotropic exchange interaction between the ground-state multiplet of one and the excited state of the other.[21] In fact, a pair of neighboring Mn^{2+} in their ${}^6S_{5/2}$ states in a magnetic field $\mathbf{H}\|\hat{\mathbf{z}}$ can be described by the Hamiltonian

$$\mathcal{H}=g\mu_B HS_z-J(S^2-\tfrac{35}{2}),$$

where J is the Mn^{2+}-Mn^{2+} exchange integral and $S=S^{(1)}+S^{(2)}$. The $5\omega_{PM}$ and $6\omega_{PM}$ will have contributions from $S=3$, 4, and 5, while the $7\omega_{PM}$ will have contributions only from $S=4$ and 5, and hence will be correspondingly weaker. Note that in the virtual transitions involving this anisotropic exchange interaction the total angular momentum need not be conserved.

2. *Spin flip from electrons bound to donors*

Another Raman feature associated with magnetic excitations encountered in DMS alloys is the spin flip of electrons bound to donors, enhanced by the *sp-d* exchange interaction. Figure 13 shows the Raman spectrum of the superlattice SL-7 (see Table III), where a Raman line consistent with spin flip is observed. The spectrum is obtained at $T=5$ K in the backscattering configuration $z(xy)\bar{z}$, with a magnetic field of 50 kG along x. As in a bulk DMS, the Raman shift of the donor spin-flip line exhibits a Brillouin-function-like behavior, as can be seen in Fig. 14. Since the spin-flip Raman mechanism also involves interband electronic transitions,[20] the observed resonant enhancement for incident frequencies close to excitonic excitations is to be expected.

The spin splitting of the donor ground state in DMS's is determined by the macroscopic magnetization of the Mn^{2+} ions and the "intrinsic" Zeeman effect, i.e.,

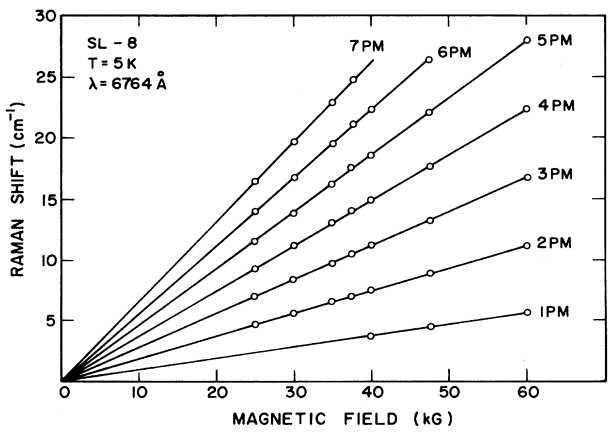

FIG. 12. Raman-EPR (PM) shift as a function of magnetic field in the $Cd_{0.9}Mn_{0.1}Se/ZnSe$ superlattice (SL-8), at $T=5$ K. The solid lines correspond to the Raman-EPR shift given by $ng_{Mn^{2+}}\mu_B H$ with $g_{Mn^{2+}}=2$ and $n=1,2,\ldots,7$.

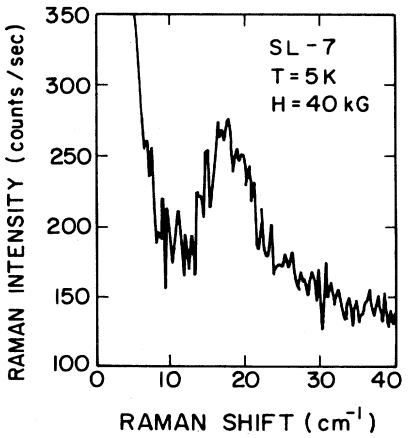

FIG. 13. Raman spectrum associated with the spin flip of electrons bound to donors in the $Cd_{0.9}Zn_{0.1}Se/Cd_{0.9}Mn_{0.1}Se$ superlattice (SL-7). The spectrum is obtained at $T=20$ K in the crossed polarization $z(yx)\bar{z}$ with $H=40$ kG along x and incident wavelength of 6471 Å.

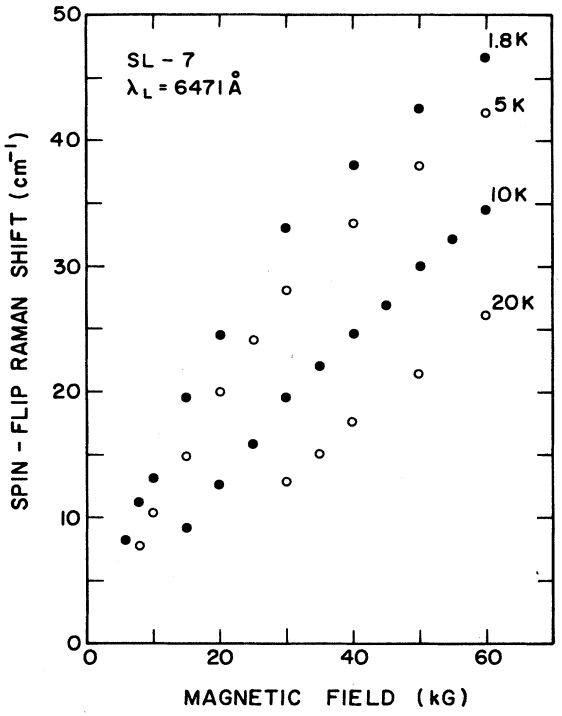

FIG. 14. Magnetic field and temperature dependence of the spin-flip Raman shift in the $Cd_{0.9}Zn_{0.1}Se/Cd_{0.9}Mn_{0.1}Se$ superlattice (SL-7) with external magnetic field in the plane of the (001) layers. The spectra were obtained in the cross polarization $z(xy)\bar{z}$ with incident laser wavelength $\lambda_L = 6471$ Å.

$$\hbar\omega_{\mathrm{SFR}} = \frac{\alpha}{g_{\mathrm{Mn}^{2+}}} M_0(H) + g^*\mu_B H = g_{\mathrm{eff}}\mu_B H \ ,$$

where α is the exchange integral characterizing the interaction between the spins of Mn^{2+} ions and those of the s-like Γ_6 electrons, μ_B the Bohr magneton, $M_0(H)$ the macroscopic magnetization, $g_{\mathrm{Mn}^{2+}} = 2$ the g factor of Mn^{2+}, g^* the intrinsic g factor of the band electrons, and g_{eff} the effective g factor of the conduction band. Because of the strong s-d exchange interaction, the first term, characterized by the Brillouin function $B_{5/2}(g\mu_B H/k_B T)$, dominates the spin splitting.[22]

From the slope of the linear portion of the spin-flip data for SL-7 shown in Fig. 14, we obtain $g_{\mathrm{eff}} = 22$ at $T = 5$ K, which is comparable to that observed in bulk $Cd_{1-y}Mn_ySe$ with $y < 0.01$, much lower than the actual value of y in this superlattice (see Table III). The reason for the smaller Raman shift observed has to be sought in terms of the magnitude of the band offset which could result in electrons being in the quantum well levels while the donors are in the barrier, the well or the interface, the Mn^{2+} ions being in the barrier. The value of y can also be estimated from the frequency of the optical phonons. The Raman spectrum of SL-7 shows peaks at 230 and 210 cm^{-1} which can be attributed to MnSe-like and CdSe-like LO modes, respectively, corresponding to the Mn^{2+} concentration of the barrier $y \sim 0.1$. A simple calculation based on a linear chain model[23] indicates that the former Raman line is a confined mode, whereas the latter is a propagating optical phonon. We should emphasize, however, that the correlation of the Raman shift with y of the barrier must also take into account the strain effects arising from the lattice mismatch. In order to estimate this, the thicknesses of the constituent layers have to be known more precisely.

IV. CONCLUDING REMARKS

The Raman-scattering studies reported in this paper confirm the zinc-blende nature of CdSe, $Cd_{1-x}Mn_xSe$, and $Cd_{1-x}Zn_xSe$ epilayers grown on (001) GaAs substrates. These new members of the family of II-VI compound semiconductors and their alloys are zinc-blende counterparts of the wurtzite structure occurring in bulk crystals. As a member of the DMS family of materials, zinc-blende $Cd_{1-x}Mn_xSe$ shows evidence of the magnetic excitations characteristic of these materials, namely Raman-EPR and spin-flip scattering from donor-bound electrons. These features are also seen in $Cd_{1-x}Mn_xSe$ layers incorporated in superlattices. As the growth parameters are brought under better control, features characteristic of superlattices and quantum wells (such as folded acoustic phonons, confined optical phonons, and confined electronic levels) will be explored.

ACKNOWLEDGMENTS

The work reported in this paper was carried out with support from the Defense Advanced Research Projects Agency–University Research Initiative Consortium on "Diluted Magnetic Semiconductors and their Heterostructures," administered by the Office of Naval Research (under contract No. N00014-86-K-0760), U.S. Department of Defense. The work at Purdue and at University of Notre Dame also received support from the National Science Foundation, Grants No. DMR-86-16787 and No. DMR-85-20866, respectively.

[1]J. K. Furdyna, J. Appl. Phys. **64**, R29 (1988).

[2]See, J. K. Furdyna and J. Kossut, in *Semiconductors and Semimentals,* edited by R. K. Willardson and A. C. Beer (Academic, New York, 1988), Vol. 25.

[3]N. Samarth, H. Luo, J. K. Furdyna, S. B. Quadri, Y. R. Lee, A. K. Ramdas, and N. Otsuka, Appl. Phys. Lett. **54**, 2680 (1989).

[4]N. Samarth, H. Luo, J. K. Furdyna, S. B. Quadri, Y. R. Lee, A. K. Ramdas, and N. Otsuka (unpublished).

[5]R. Ludeke and W. Paul, in *II-VI Semiconducting Compounds,* 1967 International Conference, edited by D. G. Thomas (Benjamin, New York, 1967), p. 123.

[6]D. L. Peterson, A Petrou, W. Giriat, A. K. Ramdas, and S. Rodriguez, Phys. Rev. B **33**, 1160 (1986).

[7]J. A. Gaj, R. R. Galazka, and M. Nawrocki, Solid State Commun. **25**, 193 (1978); D. U. Bartholomew, J. K. Furdyna, and A. K. Ramdas, Phys. Rev. B **34**, 6943 (1986); Eunsoon Oh, D.

U. Bartholomew, A. K. Ramdas, J. K. Furdyna, and U. Debska, *ibid.* **38**, 13 183 (1988).

[8]See the article by A. K. Ramdas and S. Rodriguez in Ref. 2, p. 345.

[9]DCM is an abbreviation for 4-(dicyanomethylene)-2-methyl-6-(*p*-dimethylaminostyryl)-4*H*-pyran.

[10]K. Zanio, in *Semiconductors and Semimetals,* edited by R. K. Willardson and A. C. Beer (Academic, New York, 1978), Vol. 13, p. 129.

[11]Y. R. Lee, A. K. Ramdas, and R. L. Aggarwal, Phys. Rev. B **38**, 10 600 (1988).

[12]*Semiconductors: Physics of II-VI and I-VII Compounds, Semimagnetic Semiconductors,* Vol. III/17b of *Landolt-Börnstein, New Series,* edited by K.-H. Hellwege (Springer-Verlag, Berlin, 1982).

[13]M. L. Cohen, in *II-VI Semiconducting Compounds,* 1967 International Conference, edited by D. G. Thomas (Benjamin, New York, 1967), p. 462.

[14]D. J. Stukel, R. N. Euwema, T. C. Collins, F. Herman, and R. L. Kortum, Phys. Rev. **179**, 740 (1969).

[15]R. L. Aggarwal, S. N. Jasperson, J. Stankiewicz, Y. Shapira, S. Foner, B. Khazai, and A. Wold. Phys. Rev. B **28**, 6907 (1983).

[16]A. K. Arora, E.-K. Suh, U. Debska, and A. K. Ramdas, Phys. Rev. B **37**, 2927 (1988) and A. K. Arora and A. K. Ramdas, *ibid.* **35**, 4345 (1987) for reference to the previous literature on ZnSe and CdSe, respectively.

[17]E.-K. Suh, A. K. Arora, A. K. Ramdas, and S. Rodriguez (unpublished).

[18]L. Genzel, T. P. Martin, and C. H. Perry, Phys. Status Solidi B **62**, 83 (1974).

[19]The origin of values given in Table II is as follows. The values for $\omega_{\mathrm{LO(CdSe)}}$, $\omega_{I\mathrm{(CdSe:Zn)}}$, $\omega_{I\mathrm{(ZnSe:Cd)}}$, and $\omega_{I\mathrm{(MnSe:Cd)}}$ are experimental, obtained by us at 5 K; $\omega_{\mathrm{TO(ZnSe)}}$ and $\omega_{\mathrm{LO(ZnSe)}}$ are experimental values obtained by us at 80 K in bulk crystals; $\omega_{\mathrm{TO(CdSe)}}$, $\omega_{I\mathrm{(CdSe:Mn)}}$, $\omega_{\mathrm{TO(MnSe)}}$, and $\omega_{\mathrm{LO(MnSe)}}$ are averages of the corresponding values for the A_1 and E_1 modes of wurtzite CdSe whereas ϵ_0(CdSe) is the average of $\epsilon_0^{\parallel}$ and $\epsilon_0^{\perp}$ of wurtzite CdSe (Ref. 17). The value of ϵ_0(ZnSe) is given in Ref. 12, while the value assigned to ϵ_0(MnSe) was based on the fitting of the MREI model to the experimental data in Fig. 7. For the lattice constants, a linear behavior as a function of x is assumed. The lattice constants for ZnSe and MnSe are deduced from the cation-cation distances listed in Ref. 1. The lattice constant for zinc-blende CdSe is given in Ref. 3.

[20]A. Petrou, D. L. Peterson, S. Venugopalan, R. R. Galazka, A. K. Ramdas, and S. Rodriguez, Phys. Rev. B **27**, 3471 (1983).

[21]D. L. Peterson, D. U. Bartholomew, A. K. Ramdas, and S. Rodriguez, Phys. Rev. B **31**, 7932 (1985).

[22]D. L. Peterson, D. U. Bartholomew, U. Debska, A. K. Ramdas, and S. Rodriguez, Phys. Rev. B **32**, 323 (1985).

[23]E.-K. Suh, D. U. Bartholomew, A. K. Ramdas, S. Rodriguez, S. Venugopalan, L. A. Kolodziejski, and R. L. Gunshor, Phys. Rev. B **36**, 4316 (1987).